



Wave-based room acoustic simulations of an open plan office

Huiqing Wang^{1,*}, Wouter Wittebol¹, Matthias Cosnefroy¹, Maarten Hornikx¹, Remy Wenmaekers²

¹Building Physics and Services, Department of the Built Environment, Eindhoven University of Technology,
P.O. Box 513, 5600 MB Eindhoven, The Netherlands

²Level Acoustics & Vibration, De Rondon 10, 5612 AP Eindhoven, The Netherlands

*{h.wang6@tue.nl}

Abstract

In this study, room acoustic simulations of a real open plan office using the time-domain discontinuous Galerkin (TD-DG) method are performed, as a preliminary attempt to assess the accuracy and applicability of this wave-based method for realistic sound field analysis in the low-frequency range. This TD-DG simulation involves the developed techniques of locally-reacting frequency-dependent impedance boundary conditions and the local-time stepping scheme. The required input for the boundary modeling of relevant absorption materials is obtained from the absorption coefficients measured in a reverberation room based on the international standard ISO 354. Observed discrepancies, in terms of the room acoustic parameters, between the measurements and simulation results indicate the limitation of the detailed wave-based modeling in the absence of a precise boundary characterization.

Keywords: wave-based simulation, time-domain discontinuous Galerkin method, open-plan office.

1 Introduction

Wave-based room acoustic simulation methods simulate sound propagation by directly solving the wave equation based on numerical approximation techniques. Compared to the well-established geometrical acoustic (GA) simulation techniques [1], which are built upon the assumption that sound acts as rays, wave-based methods are able to accurately capture inherent complex wave-phenomena such as scattering, diffraction and phase effects. Despite their superior accuracy, wave-based methods suffer from a heavy computational cost. Therefore, GA simulation methods have been the prevailing approach for acoustic practitioners and researchers for simulating the acoustic fields of large rooms like concert halls and theaters; while it is generally acknowledged that wave-based methods serve as preferred alternatives to GA models for rooms with small volumes below the Schroeder frequency, where the modal overlap is low. Recently, the time-domain discontinuous Galerkin (TD-DG) wave-based method has been investigated for room acoustic modeling purposes [2, 3] and efforts have been made to enhance its performance in terms of acoustic boundary modeling [2, 4, 5], efficiency [6] and high-performance computing [2].

A comprehensive evaluation of the accuracy of room acoustic simulations typically involves a comparison with measurements. For state-of-the-art of room acoustic modeling software that are based on GA models, round robin experiments have been performed using acoustic scenes of different levels of complexity [7] and benchmark databases have been established [8]. Audible deviations are observed, and it proves to be a challenging task to guarantee an exact match of model input parameters between simulations and measurements. Sources of input data uncertainties include room geometries, absorption and scattering properties of room surfaces and the source and receiver characteristics [9].

For wave-based methods, there have been on-going research activities trying to close the gap between real-world measurements and simulations as well. Experimental validation of room acoustic simulations inside a reverberation room with a time-domain finite element method (FEM) is reported by Okuzono *et al.*

[10], and a decent agreement of band-limited room impulse responses is observed in three separate octave bands. Comparisons of different boundary representations of porous absorbers in small rooms are performed respectively within the framework of the frequency-domain FEM model [11] and the TD-DG model [12], highlighting the effects of extended reaction of boundary materials for room acoustics. For the TD-DG method, previous validation work [3] has been done inside an empty reverberation room, where the walls are modeled with a uniform real-valued impedance. Later on, benchmark tests with various furniture inside were conducted [13] and the good match with measurements indicate the strong potential for more challenging and larger room scenarios. Another recent study compares measurements with simulation results from the TD-DG method in a small rectangular room with porous absorbers, with a focus on establishing a comprehensive validation and uncertainty quantification framework in wave-based room acoustic simulations [14]. It was found that the input uncertainties associated with the absorption properties makes it intractable to predict common room acoustic parameters within just noticeable difference (JND) thresholds.

In this study, the TD-DG method is applied to simulate the acoustics of a large real open plan office in the low-to-middle frequency range (125 Hz to 500 Hz octave bands), with the aim of assessing the accuracy and applicability of this wave-based method for realistic sound field analysis. The ground truth references to be compared with are measurement results, which were previously published in a study on how room acoustic parameters are affected with varying configurations of furniture and sound absorbing barriers [15]. The acoustic properties of involved boundary surfaces are characterized based on standardized reverberation room measurements [16]. The required specifications of complex-valued reflection coefficients for the wave-based calculations are obtained by transforming the measured Sabine absorption coefficients. The comparison between the simulation and measurement results are conducted in terms of six room acoustic parameters that are derived from the room impulse response.

The paper is organized as follows. The description of the reference room measurements is presented in Sec. 2. Sec. 3 describes the setup of the wave-based simulation model and the approach used for retrieving complex-valued impedance boundary data. Section 4 presents the comparison of simulation results with measurements, as well as discussions on the potential limitations of the current wave-based model.

2 Reference measurement

2.1. Measurement room and procedures

As shown in Fig. 1, the open plan office under study has a long and narrow floor plan with windows along the walls. Small closed rooms indicated by the blue areas are present to subdivide the long space. The room has a volume of 962 m³ and the ceiling is 2.9 m tall. During the measurements, the room was completely empty except for the 5 workstation islands. Within each group of 4 workstations, two variations of the setup are considered:

- V1: only tables in the room,
- V2: tables with dividing panels and side panels.

The source location and the 9 receiver locations are denoted by the red and yellow circles respectively, with the exact position of the source and of one receiver (R_9) provided. The table depth for each sitting position is 0.8 m and the source and microphones are positioned 0.3 m away from the tables. More geometrical details can be found in Ref. [15]. The measurements have been performed following ISO 3382-3 [17]. An omnidirectional sound source (B&K 4292) and omnidirectional microphones were connected to a laptop with measurement software Dirac 6 (B&K 7841) via a triton USB device (AE) and an amplifier (B&K 2734).

2.2. Acoustic properties of room materials

The room has a sound absorbing suspended ceiling of 20 mm thick Rockfon panels with an air cavity of at least 200 mm. The floor is covered with carpet. Dividing and side panels, which are made of 25 mm chipboard,

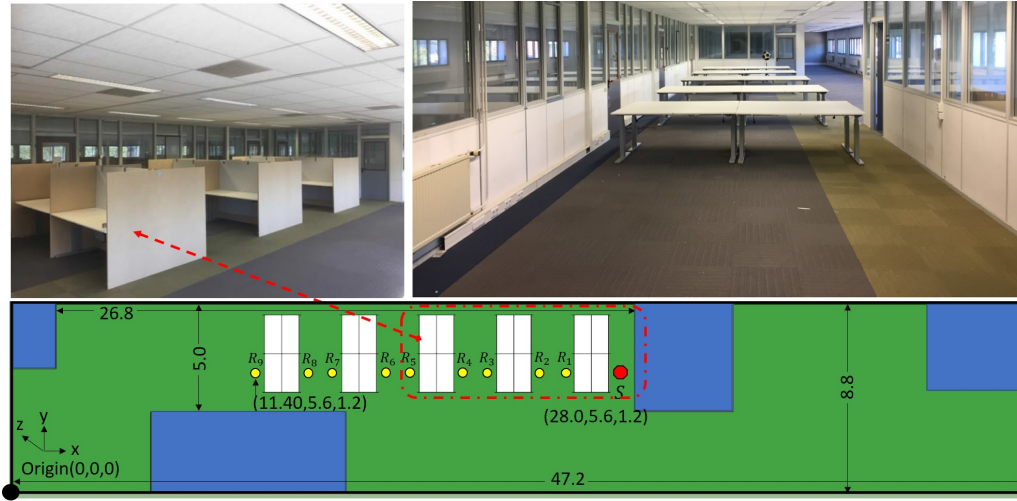


Figure 1: Pictures of the measured open plan office and its floor plan in top view.

stand on the floor and have a height of 1.5 m. To increase sound absorption, 30 mm thick melamine foam is applied to both sides of the upper 1.3 m part of the dividing panels that are along the y-direction. The acoustic properties of the room surface materials, which are represented with the Sabine absorption coefficients in this work, are measured in a reverberation chamber according to ISO354 [16] and are available in octave bands as shown in Table 1. The Sabine absorption coefficients are measured by the reverberation chamber method as follows:

$$\alpha_{Sab} = \frac{55.3V}{S c_0} \left(\frac{1}{T_2} - \frac{1}{T_1} \right), \quad (1)$$

where V is the volume of the reverberation chamber, S is the area of the material sample, T_1 is the reverberation

Table 1: Measured Sabine absorption coefficients α_{Sab} of materials in octave bands. The values in parentheses are the estimated size-corrected ones used in simulations, as described in Sec. 3

Frequency [Hz]/Materials	Ceiling	Foam	Carpet
125	0.45 (0.45)	0.10 (0.11)	0.02 (0.01)
250	0.70 (0.72)	0.35 (0.33)	0.03 (0.03)
500	0.90 (0.87)	0.60 (0.62)	0.07 (0.08)

time for an empty condition, and T_2 is the reverberation time with the test sample. It should be mentioned that due to the limited volume of the reverberation chamber, the measurements for the suspended ceiling are performed with the mounting type E-200 of ISO 354 [16], *i.e.*, placing the test sample with a 200 mm cavity behind it.

3 Wave-based modeling

3.1. Brief description of the time-domain DG method

The simulations are performed using an in-house simulation tool based on the TD-DG method. This section presents the main formulations whereas additional details can be found in Refs. [3, 4, 6]. Under the assumption of lossless propagation medium, the sound propagation is governed by the following partial differential equations

$$\frac{\partial \mathbf{q}}{\partial t} + \nabla \cdot \mathbf{F}(\mathbf{q}) = \frac{\partial \mathbf{q}}{\partial t} + \mathbf{A}_j \frac{\partial \mathbf{q}}{\partial x_j} = \mathbf{0}, \quad (2)$$

where $\mathbf{q}(\mathbf{x}, t) = [u, v, w, p]^T$ is the acoustic variable vector, containing the particle velocity component $[u, v, w]$ and the sound pressure p . ρ is the constant air density and c is the constant speed of sound. The constant flux Jacobian matrix \mathbf{A}_j reads

$$\mathbf{A}_j = \begin{bmatrix} 0 & 0 & 0 & \frac{\delta_{xj}}{\rho} \\ 0 & 0 & 0 & \frac{\delta_{yj}}{\rho} \\ 0 & 0 & 0 & \frac{\delta_{zj}}{\rho} \\ \rho c^2 \delta_{xj} & \rho c^2 \delta_{yj} & \rho c^2 \delta_{zj} & 0 \end{bmatrix}, \quad (3)$$

with coordinate index $j \in [x, y, z]$. Let D^k be a set of simplex and geometrically conformal elements that discretize the computational domain Ω_h , *i.e.*, $\Omega_h = \bigcup_{k=1}^K D^k$. The local solution $\mathbf{q}_h^k(\mathbf{x}, t)$ in element D^k , where subscript h denotes the numerical approximation, is given by:

$$\mathbf{q}_h^k(\mathbf{x}, t) = \sum_{i=1}^{N_p} \mathbf{q}_h^k(\mathbf{x}_i^k, t) l_i^k(\mathbf{x}), \quad (4)$$

where $\mathbf{q}_h^k(\mathbf{x}_i^k, t)$ are the unknown nodal values and $l_i^k(\mathbf{x})$ is the multi-dimensional Lagrange polynomial basis of order N , which satisfies $l_i^k(\mathbf{x}_j^k) = \delta_{ij}$. N_p is the number of local basis functions (or nodes) inside a single element and is equal to $(N+d)!/(N!d!)$ for simplex elements, where d is the dimensionality. After the Galerkin projection and integrating by parts twice, the semi-discrete nodal DG formulation of Eq. (2) reads:

$$\int_{D^k} \left(\frac{\partial \mathbf{q}_h^k}{\partial t} + \nabla \cdot \mathbf{F}_h^k(\mathbf{q}_h^k) \right) l_i^k d\mathbf{x} = \int_{\partial D^k} \mathbf{n} \cdot \left(\mathbf{F}_h^k(\mathbf{q}_h^k) - \mathbf{F}^* \right) l_i^k d\mathbf{x}, \quad (5)$$

where $\mathbf{n} = [n_x, n_y, n_z]$ is the outward normal vector of the element surface ∂D^k . \mathbf{F}^* is the numerical flux across element intersection ∂D^k and in this study, the upwind numerical flux is used throughout the whole domain because of its low dispersive and dissipation error. The semi-discrete formulation is obtained by substituting the nodal basis expansion Eq. (4) into the strong formulation Eq. (5). The resulting vector-matrix form of the formulation and more details of the implementation can be found in Ref. [3].

Locally reacting time-domain impedance boundary conditions (TDIBC) are weakly enforced through the numerical flux terms, where the reflected characteristic wave is expressed as the convolution between the reflection coefficient at normal incidence and the incident characteristic wave. The method of auxiliary differential equations is used to calculate the convolution. The reflection coefficient is represented by the multi-pole model as described in Ref. [4].

The semi-discrete system with a 6th order spatial approximation is integrated in time using a 5th order explicit Taylor series integrator based on the arbitrary high-order derivatives (ADER) methodology, with a local time-stepping scheme incorporated as presented in [6].

3.2. Mesh generation

The model geometry is imported into the meshing software Gmsh [18] to generate the unstructured tetrahedral mesh, as shown in Fig. 2 for the V2 setup. The geometrical model contains all details whose dimensions are comparable to the shortest wavelength resolved, which is around 0.5 m. The absorbing foam, dividing panels and desks are modeled as “floating” surfaces with their thicknesses neglected.

It is known that the mesh quality has a pivotal influence on the maximum allowable time step size and the numerical error. In Gmsh, mesh element sizes are usually prescribed by adjusting the so-called characteristic lengths (denoted as L_c), which are more or less equal to the length of the element edges. Here, the radius of the largest inscribed sphere r_{in} is used as the element size measure. The chosen quality measure r_q is triple of the ratio between r_{in} and the radius of the smallest circumscribed sphere r_{cir} , *i.e.* $r_q = 3r_{in}/r_{cir}$. As a reference, a regular tetrahedron has $r_q = 1$ (optimal mesh quality), and a degenerate tetrahedron (zero volume) has $r_q = 0$. Considering the maximum frequency of interest of 500 Hz, meshes with five different

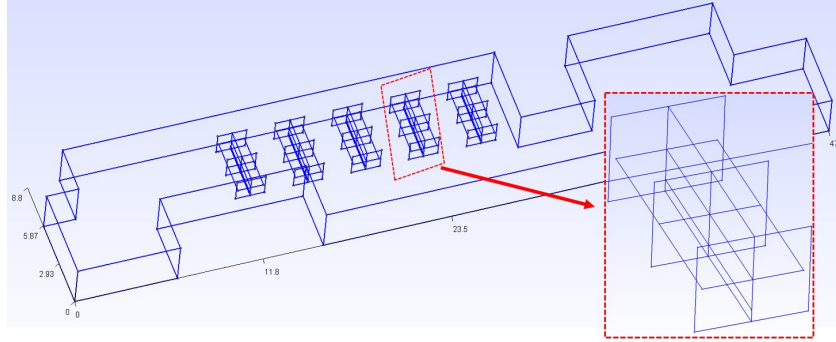


Figure 2: Geometry model in Gmsh.

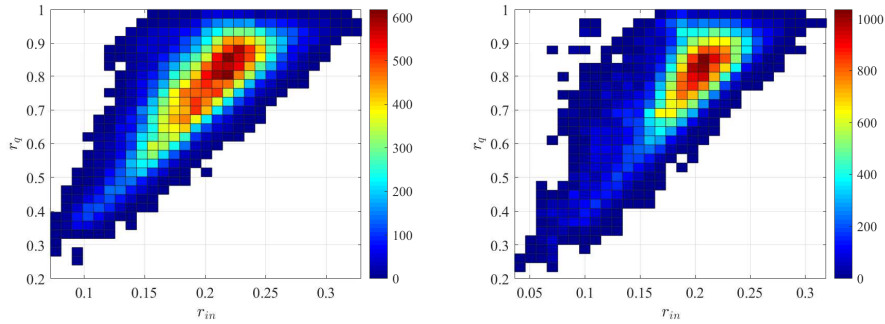


Figure 3: Distribution of the mesh quality measure r_q and the mesh size measure r_{in} . V1 and V2 are displayed in the left and right plot respectively. The color indicates the number of elements in each bin.

$L_c = [0.3, 0.35, 0.4, 0.45, 0.5]$ m values are generated for both setups. It is found that decreasing the mesh element size (increasing the number of elements) does not necessarily yield larger values of r_q (better mesh quality). By comparing the distributions of the mesh quality measure r_q and the element size measure r_{in} , the meshes with $L_c = 0.45$ m are chosen for both setups, with their distributions of r_q and r_{in} are shown in Fig. 3. The number of elements are 50379 and 57489 for V1 and V2, respectively. The points per wavelength is 11.2 (11.8) at the center frequency and 7.9 (8.3) at the upper limit of 500 Hz octave band for the V1 (V2) mesh. In this work, considering the CFL stability condition of the explicit time integration scheme, the time step size is determined by

$$\Delta t = C_{CFL} \cdot \min(r_{in}) \cdot \frac{1}{c} \cdot \frac{1}{(2N + 1)}. \quad (6)$$

In this study, C_{CFL} is set to 0.9, and $\min(r_{in}) = 0.074$ m for V1 and $\min(r_{in}) = 0.042$ m for V2. To accelerate the simulation for the V2 setup, where small elements exist around the corner of table dividers due to the geometry constraint, a local time-stepping scheme [6] is used and all elements are divided into two groups. All elements that have $r_{in} \leq 3 \min(r_{in})$ are marked as fine elements, accounting for 8.4% of total elements, and are time integrated with Δt of Eq. (6). The rest are considered as coarse elements and have a time step size of $3\Delta t$.

3.3. Acoustic boundary modeling

The measured Sabine absorption coefficients α_{Sab} are energy parameters that do not carry phase information. They approximately represent the theoretical random incidence absorption coefficient α_{rand} for plane wave incidence on an infinitely large surface. However, for wave-based room acoustic simulations, such as the TD-DG method herein, the complex-valued surface impedances or equivalent reflection coefficients are needed for the boundary modeling. In general, it is considered intractable to retrieve the correct complex-valued surface impedance from a real-valued absorption coefficient when there is no more information on the material

available, because there are an infinite number of surface impedance values that yield the same absorption coefficient. To address this issue, a common strategy is to add some assumptions and constraints [19, 20]. First of all, local reaction is assumed, meaning that the surface impedance $Z_s(\theta)$ is independent of the angle of incidence θ (and thus the surface impedance for normal incidence is assumed representative of all incidence angles). Secondly, as proposed in Refs. [21, 20], we assume that the measured Sabine absorption coefficient corresponds to the size-corrected absorption coefficient for the low frequency range of interest, which is proposed by Thomasson [22] as follows:

$$\alpha_{size}(\theta) = 8 \int_0^{\pi/2} \frac{\text{Re}(Z_s(\theta)) \sin \theta}{|Z_s(\theta) + \bar{Z}_r(\theta)|^2} d\theta, \quad (7)$$

where \bar{Z}_r is the averaged radiation impedance over azimuthal angles ϕ and expressed as $\bar{Z}_r = \int_0^{2\pi} Z_r d\phi / 2\pi$. The average radiation impedance can be calculated with numerical integrations in an accurate way, based on tabulated values provided in Table I of Ref. [21].

From the rudimentary assessment of the limited absorption coefficients data, the rigidly-backed foam and carpet correspond to the cases “soft porous” and “hard porous” as discussed in Ref. [20]. It has been shown therein that the surface impedance of rigidly-backing porous materials, which exhibits a monotonic behavior, can be well captured by approximations with fractional derivatives, similar to the multi-pole model representation as used in the TDIBC here. By contrast, the suspended ceiling with a large air cavity is quite difficult to simulate in practice [20], because the cotangent term in the surface impedance produces oscillating behavior. Therefore, the resulting narrow-band frequency variations are impossible to be reasonably captured from the coarse frequency-averaged octave band data. In this work, restricted by the availability of input data, we preliminarily assume that strong oscillations are not present in the current frequency range of interest. The multi-pole parameters needed for the TDIBC are determined by solving an optimization problem. The idea is to optimize the parameters in the multi-pole approximations of the reflection coefficient at normal incidence (denoted as R_{nor}), which can be linearly transformed into the surface impedance in Eq. (7), that produces the best match between the measured and the estimated size-corrected absorption coefficient. The magnitude and the phase angle of fitted reflection coefficients R_{nor} are shown in Fig. 4. The corresponding size-corrected absorption coefficients are the values inside the parenthesis of Table 1.

Besides the considered ceiling, foam and carpet, there are other materials in the room absorbing sound in

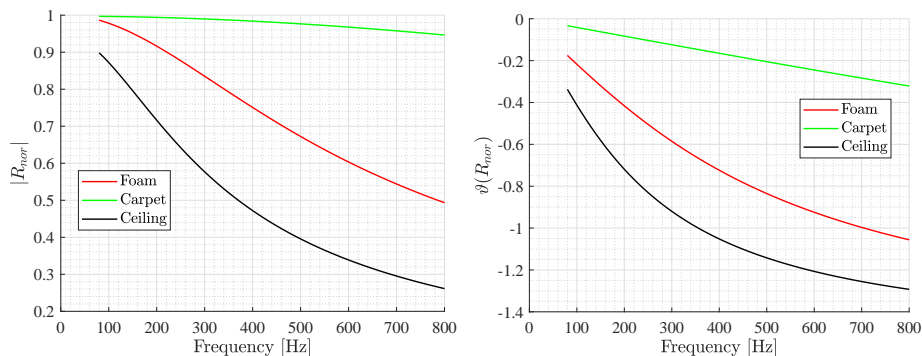


Figure 4: Estimated reflection coefficient at normal incidence. $\vartheta(\cdot)$ extracts the phase angle of a complex number.

the considered frequency range, for example the window glass and gypsum board. However, the detailed information on their sizes and acoustic properties are missing. Here, real-valued impedances in octave bands are assigned to all other surfaces in the room guided by the typical values of absorption coefficients provided in Ref. [23], *i.e.*, 0.15, 0.15 and 0.1 for the octave bands 125 Hz, 250 Hz and 500 Hz respectively.

Table 2: Spatial average of the considered room acoustic parameters and their standard deviation for both setups. The values before the slash are the measured ones and after the slash are the simulated ones.

Para.	Oct.	Space aver. V1	Std. V1	Space aver. V2	Std. V2
T_{30} [s]	125	0.83/0.70	0.06/0.08	0.78/0.61	0.09/0.08
	250	0.80/1.14	0.07/0.20	0.76/0.82	0.14/0.12
	500	0.64/1.13	0.07/0.26	0.61/0.79	0.10/0.08
EDT [s]	125	0.70/0.79	0.26/0.31	0.94/0.92	0.33/0.33
	250	0.57/0.78	0.18/0.21	0.77/0.68	0.22/0.25
	500	0.55/0.83	0.20/0.29	0.61/0.69	0.21/0.28
C_{50} [dB]	125	4.70/3.0	3.10/4.94	-0.47/0.34	5.24/2.98
	250	6.50/4.75	2.54/1.66	2.02/5.65	2.89/4.71
	500	6.80/3.31	3.26/3.00	6.25/4.23	3.32/2.71
T_S [ms]	125	77.5/79.0	25.9/33.7	100.9/99.1	35.4/33.7
	250	66.2/77.8	23.6/28.2	88.7/75.5	28.5/29.0
	500	59.2/80.6	25.3/32.8	70.9/76.0	24.7/28.3

4 Results

The results from the measurements and the simulations are first evaluated in terms of standard room acoustic parameters as stated in ISO 3382-1 [24], including reverberation time (T_{30}), early decay time (EDT), clarity (C_{50}) and center of gravity (T_S). In the DG simulation, the dodecahedron source is modeled by a point source that has a Gaussian shaped time signal with a non-flat spectrum. Therefore, the simulated responses are deconvolved by the spectral division approach with the water level regularization technique [25] applied in order to get the room impulse responses.

In order to evaluate room acoustic parameters that are representative of the whole room, the spatial averaging values, which are obtained from the arithmetic average for all nine receiver locations, are presented in Table 2. The standard deviations provide insights into the spatial variance of the parameters across various locations. The first impression of the comparison results is that none of the simulation results match the measured ones very well, except for the center time T_S at 125 Hz, which is the center of gravity of the squared impulse response and indicates the balance between clarity and reverberance. Larger deviations are observed for spatial mean values of both T_{30} and EDT , which are directly calculated from the energy decay curve. For T_{30} , lower values are predicted compared to the measurements for both setups in the 125 Hz octave band, whereas higher values are found in the simulations for the 250 Hz and 500 Hz octave bands. For the clarity C_{50} , the simulated values are lower than the measured ones, except for setup V2 at 125 Hz, implying that the simulated sound field is more perceptually blurred.

The reverberation time of a room is usually regarded as the predominant indicator of its acoustical properties. However, for the open plan office, good speech privacy between workstations is of primary concern. Therefore, the spatial decay rate of speech $D_{2,S}$ (level reduction when doubling the distance) and A-weighted sound pressure level (SPL) of speech at a distance of 4 m from the sound source ($L_{p,A,S,4m}$) as described in ISO 3382-3 [17] are investigated. The sound power level of the loud speaker and simulation impulse source are normalized based on the SPL at a distance of 1 m in the free-field condition. Due to the limited frequency range of the wave-based simulations, the logarithm summation of the A-weighted SPL is calculated only up to the 500 Hz octave band instead of 8000 Hz for both simulation and measurements. It should be noted that due to the SPL spectrum of normal speech and the A-weighting, the A-weighted SPL of speech almost fully depends on the 500 Hz octave band.

The comparisons for the V1 setup (with empty tables alone) and the V2 setup (with table dividers and side panels) are shown in Fig. 5, where the linear regression is performed to determine $D_{2,S}$ according to ISO 3382-3 [17]. It can be seen that the simulations have a lower predicted SPL of normal speech for all receiver locations except the eighth receiver. The discrepancies get smaller at further distance. Furthermore, the simulated spatial decay rates of speech $D_{2,S}$ are smaller than the measured ones in both cases. For the V1 setup, the monotonic decrease of $L_{p,A,S}$ is well predicted, while a fairly good agreement of the zigzag shape in terms of $L_{p,A,S}$ is observed for the V2 setup, implying the effects of the table dividers and side panels are taken into account in the simulations.

The considered comparison has proven to be quite challenging. While it is intractable to pin down the exact

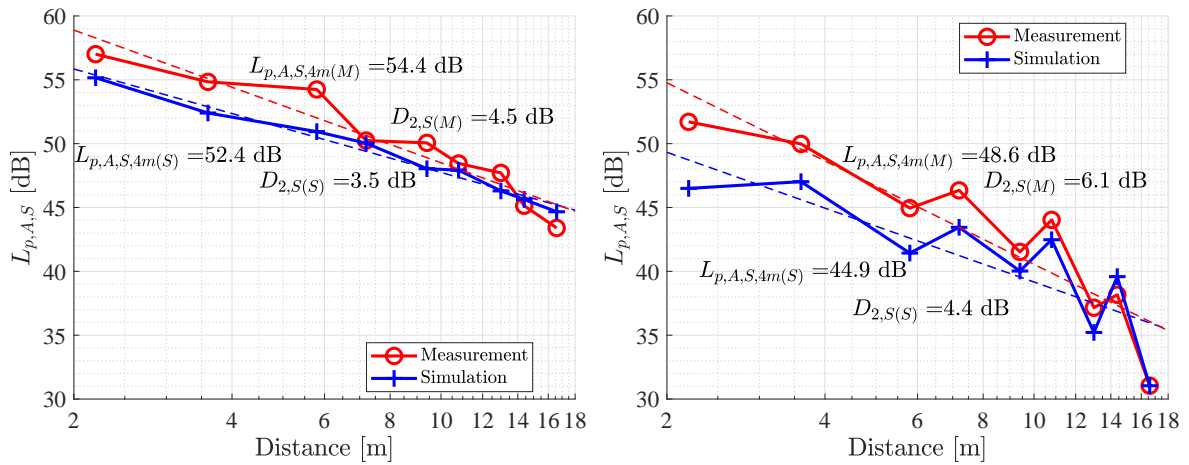


Figure 5: Comparison of $D_{2,S}$ and $L_{p,A,S,4m}$. V1 and V2 are displayed in the left and right plot respectively.

deficiency of the numerical model, the discrepancies between the simulation and measurement results can be elucidated mainly from the following three aspects. First of all, there are inevitable uncertainties and inherent randomness in both the measurements and the simulation inputs, including boundary material properties, geometry and the source/receiver locations. In this study, the lack of knowledge about the exact size of the windows and their acoustic properties could also affect the accuracy of simulated T_{30} and EDT .

Secondly, the measured absorption coefficients of three major absorbing materials according to ISO 354 [16] may not truly represent the acoustic properties of the materials due to the limitation of the standard [26, 27]. Furthermore, octave band data does not provide a sufficient frequency resolution for simulation purposes. The acoustic properties of the considered materials might not be monotonic in the interested frequency range, as assumed. Also, the accurate phase information about the surface impedance is missing, which has been shown quite influential in capturing the frequency shift [28] and the reverberation time [29]. This argument is supported by the fact that the standard deviation of EDT is slightly larger than that of T_{30} , since EDT is more sensitive to the relatively sparse early reflections.

Last but not least, the current wave-based simulation models all surfaces as locally reacting. In many applications, this assumption has prevailed due to its simplicity. However, previous studies showed that for grazing incidence waves, considerable discrepancies between locally and extendedly reacting absorbers exist [30]. For the studied office, the distance between the floor and the absorbing ceiling is rather low. As a consequence, grazing incidence might be more pronounced in the early reflections for certain source-receiver positions, resulting in a serious degradation of the accuracy in EDT . Furthermore, extended reaction most likely arises in the suspended ceiling treatment, which has an air gap larger than 200 mm. It has been shown that absorbers with an air gap exhibit strong extendedly reacting behavior and that a better agreement at larger incidence angles at lower frequencies is observed for extended reaction models [31].

5 Conclusion

Wave-based room simulation of a real open plan office in the low-frequency range has been performed with the time-domain discontinuous Galerkin method. The acoustic properties of materials are represented with the energy-based absorption coefficients in octave bands measured with the reverberation chamber method. From this input data, the needed complex-valued surface impedance data is retrieved by fitting the size-corrected Sabine absorption coefficients, assuming monotonic absorption behavior within the interested frequency range. To assess the validity of the whole framework, the simulation results are compared with the measurements in terms of room acoustic parameters.

Noticeable discrepancies between the simulation and measurement results are observed, especially for the reverberation time and early decay time. While it is generally difficult to determine which influencing factors contribute the most to the overall simulation deviations, the potential limitations of the current numerical model are summarized. It should be noted that this work is a preliminary attempt to investigate the applicability for challenging practical cases, where a high level of complexity and uncertainty in model inputs is involved. As future work, experimental validations with increasing level of complexity of room scenarios will be performed. Furthermore, the formulation of extendedly reacting boundary conditions should help to achieve satisfactory improvements in the simulation accuracy.

References

- [1] Lauri Savioja and U. Peter Svensson. Overview of geometrical room acoustic modeling techniques. *The Journal of the Acoustical Society of America*, 138(2):708–730, aug 2015.
- [2] Finnur Pind. *Wave-Based Virtual Acoustics*. PhD thesis, Technical University of Denmark, 2020.
- [3] Huiqing Wang, Indra Sihar, Raúl Pagán Muñoz, and Maarten Hornikx. Room acoustics modelling in the time-domain with the nodal discontinuous Galerkin method. *The Journal of the Acoustical Society of America*, 145(4):2650–2663, 2019.
- [4] Huiqing Wang and Maarten Hornikx. Time-domain impedance boundary condition modeling with the discontinuous Galerkin method for room acoustics simulations. *The Journal of the Acoustical Society of America*, 147(4):2534–2546, 2020.
- [5] Huiqing Wang, Jieun Yang, and Maarten Hornikx. Frequency-dependent transmission boundary condition in the acoustic time-domain nodal discontinuous Galerkin model. *Applied Acoustics*, 164:107280, 2020.
- [6] Huiqing Wang, Matthias Cosnefroy, and Maarten Hornikx. An arbitrary high-order discontinuous Galerkin method with local time-stepping for linear acoustic wave propagation. *The Journal of the Acoustical Society of America*, 149(1):569–580, 2021.
- [7] Fabian Brinkmann, Lukas Aspöck, David Ackermann, Steffen Lepa, Michael Vorländer, and Stefan Weinzierl. A round robin on room acoustical simulation and auralization. *The Journal of the Acoustical Society of America*, 145(4):2746–2760, 2019.
- [8] Fabian Brinkmann, Lukas Aspöck, David Ackermann, Rob Opdam, Michael Vorländer, and Stefan Weinzierl. A benchmark for room acoustical simulation. concept and database. *Applied Acoustics*, 176:107867, 2021.
- [9] Michael Vorländer. Computer simulations in room acoustics: Concepts and uncertainties. *The Journal of the Acoustical Society of America*, 133(3):1203–1213, mar 2013.
- [10] Takeshi Okuzono, Toru Otsuru, Reiji Tomiku, and Noriko Okamoto. Fundamental accuracy of time domain finite element method for sound-field analysis of rooms. *Applied Acoustics*, 71(10):940–946, 2010.
- [11] Marc Aretz and Michael Vorländer. Efficient modelling of absorbing boundaries in room acoustic FE simulations. *Acta Acustica united with Acustica*, 96(6):1042–1050, 2010.

- [12] Finnur Pind, Cheol-Ho Jeong, Allan P Engsig-Karup, Jan S Hesthaven, and Jakob Strømmand-Andersen. Time-domain room acoustic simulations with extended-reacting porous absorbers using the discontinuous Galerkin method. *The Journal of the Acoustical Society of America*, 148(5):2851–2863, 2020.
- [13] Fotis Georgiou, Baltazar Briere de la Hossieraye, Maarten Hornikx, and Philip W Robinson. Design and simulation of a benchmark room for room acoustic auralizations. In *23rd International Congress on Acoustics*, pages 723–730, 2019.
- [14] Tobias Thydal, Finnur Pind, Cheol-Ho Jeong, and Allan P Engsig-Karup. Experimental validation and uncertainty quantification in wave-based computational room acoustics. *Applied Acoustics*, 178:107939, 2021.
- [15] Remy Wenmaekers and Nicole van Hout. How ISO 3382-3 acoustic parameter values are affected by furniture, barriers and sound absorption in a typical open plan office. In *23rd International Congress on Acoustics*, pages 2437–2444, 2019.
- [16] ISO354: 2003. Acoustics - Measurement of sound absorption in a reverberation room. Standard, International Organization for Standardization, Geneva, CH, 2003.
- [17] ISO 3382-3. Acoustics - Measurement of room acoustic parameters - Part 3: Open plan offices. Standard, International Organization for Standardization, Geneva, CH, 2017.
- [18] Christophe Geuzaine and Jean-François Remacle. Gmsh: A 3-D finite element mesh generator with built-in pre-and post-processing facilities. *International Journal for Numerical Methods in Engineering*, 79(11):1309–1331, 2009.
- [19] Jens Holger Rindel. An impedance model for estimating the complex pressure reflection factor. In *Forum Acusticum*, volume 2011, 2011.
- [20] Boris Mondet, Jonas Brunskog, Cheol-Ho Jeong, and Jens Holger Rindel. From absorption to impedance: Enhancing boundary conditions in room acoustic simulations. *Applied Acoustics*, 157:106884, 2020.
- [21] Cheol-Ho Jeong. Converting sabine absorption coefficients to random incidence absorption coefficients. *The Journal of the Acoustical Society of America*, 133(6):3951–3962, 2013.
- [22] Sven-Ingvar Thomasson. On the absorption coefficient. *Acta Acustica united with Acustica*, 44(4):265–273, 1980.
- [23] H. Kuttruff. *Acoustics: An Introduction*. CRC Press, New York, 2006.
- [24] ISO 3382-1. Acoustics - Measurement of room acoustic parameters - Part 1: Performance spaces. Standard, International Organization for Standardization, Geneva, CH, March 2015.
- [25] *Deconvolution, a glimpse ahead*, pages 103–107. Springer Berlin Heidelberg, Berlin, Heidelberg, 1994.
- [26] Martijn Vercammen. On the revision of ISO 354, measurement of the sound absorption in the reverberation room. In *23rd International Congress on Acoustics*, pages 3991–3997, 2019.
- [27] Cheol-Ho Jeong and Ji-Ho Chang. Reproducibility of the random incidence absorption coefficient converted from the sabine absorption coefficient. *Acta Acustica united with Acustica*, 101(1):99–112, 2015.
- [28] Diego M Murillo, Filippo M Fazi, and Jeremy Astley. Room acoustic simulations using the finite element method and diffuse absorption coefficients. *Acta Acustica united with Acustica*, 105(1):231–239, 2019.
- [29] Cheol-Ho Jeong, Doheon Lee, Sébastien Santurette, and Jeong-Guon Ih. Influence of impedance phase angle on sound pressures and reverberation times in a rectangular room. *The Journal of the Acoustical Society of America*, 135(2):712–723, 2014.
- [30] Behrooz Yousefzadeh and Murray Hodgson. Energy-and wave-based beam-tracing prediction of room-acoustical parameters using different boundary conditions. *The Journal of the Acoustical Society of America*, 132(3):1450–1461, 2012.
- [31] Krístrún Gunnarsdóttir, Cheol-Ho Jeong, and Gerd Marbjerg. Acoustic behavior of porous ceiling absorbers based on local and extended reaction. *The Journal of the Acoustical Society of America*, 137(1):509–512, 2015.